

# OH regeneration from methacrolein oxidation investigated in the atmosphere simulation chamber SAPHIR

H. Fuchs<sup>1</sup>, I.-H. Acir<sup>1</sup>, B. Bohn<sup>1</sup>, T. Brauers<sup>1</sup>, H.-P. Dorn<sup>1</sup>, R. Häsel<sup>1</sup>,  
A. Hofzumahaus<sup>1</sup>, F. Holland<sup>1</sup>, M. Kaminski<sup>1</sup>, X. Li<sup>1</sup>, K. Lu<sup>1,\*</sup>, A. Lutz<sup>2</sup>,  
S. Nehr<sup>1,\*\*</sup>, F. Rohrer<sup>1</sup>, R. Tillmann<sup>1</sup>, R. Wegener<sup>1</sup>, and A. Wahner<sup>1</sup>

<sup>1</sup>Institute of Energy and Climate Research, IEK-8: Troposphere, Forschungszentrum Jülich GmbH,  
Jülich, Germany

<sup>2</sup>Institute of Chemistry and molecular Biology, Göteborg University, Göteborg, Sweden

\* now at: College of Environmental Sciences and Engineering, Peking University, Beijing, China

\*\* now at: Verein Deutscher Ingenieure e.V., Kommission Reinhaltung der Luft, Düsseldorf,  
Germany

*Correspondence to:* Hendrik Fuchs  
(h.fuchs@fz-juelich.de)


**Abstract.** Hydroxyl radicals (OH) are the most important reagent for the oxidation of trace gases in the atmosphere. OH concentrations measured during recent field campaigns in isoprene rich environments were unexpectedly large. A number of studies showed that unimolecular reactions of organic peroxy radicals (RO<sub>2</sub>) formed in the initial reaction step of isoprene with OH play an important role for the OH budget in the atmosphere at low mixing ratios of nitrogen monoxide (NO) of less than 100 pptv. It has also been suggested that similar reactions potentially play an important role for RO<sub>2</sub> from other compounds. Here, we investigate the oxidation of methacrolein (MACR), one major oxidation product of isoprene, by OH in experiments in the simulation chamber SAPHIR under controlled atmospheric conditions. The experiments show that measured OH concentrations are approximately 50 % larger than calculated by current chemical models for conditions of the experiments (NO mixing ratio of 90 pptv). The analysis of the OH budget reveals a so far unaccounted OH source, which is correlated with the production rate of RO<sub>2</sub> radicals from MACR. In order to balance the measured OH destruction rate, (0.77 ± 0.31, 1σ error) OH radicals need to be additionally reformed from each OH that has reacted with MACR. The strong correlation of the missing OH source with the production of RO<sub>2</sub> radicals is consistent with the concept of OH formation from unimolecular isomerization and decomposition reactions of RO<sub>2</sub>. The comparison of observations with model calculations gives a lower limit of 0.03 s<sup>-1</sup> for the reaction rate constant, if the OH source is attributed to an isomerization reaction of MACR-1-OH-2-OO and MACR-2-OH-2-OO formed in the MACR+OH reaction as suggested in literature (Crouse et al., 2012). This fast isomerization reaction would be competitive to the reaction of this RO<sub>2</sub>

species with minimum 150 pptv NO. The isomerization reaction would be the dominant reaction pathway for this specific RO<sub>2</sub> radical in forested regions, where NO mixing ratios are typically much smaller.

## 1 Introduction

25 Isoprene (2-methyl-1,3-butadiene) is the most abundant nonmethane hydrocarbon that is being emitted by the biosphere and predominantly removed by oxidation with atmospheric hydroxyl radicals (OH) (Guenther et al., 2012). Unexpectedly large OH concentrations that cannot be explained by the current knowledge of atmospheric chemistry have been found in several field campaigns (Carslaw et al., 2001; Tan et al., 2001; Kuhn et al., 2007; Ren et al., 2008; Lelieveld et al., 2008; Hofzumahaus et al., 2009; Lu et al., 2012, 2013; Stone et al., 2010; Whalley et al., 2011; Wolfe et al., 2011) for high loads of OH reactants (often dominated by isoprene) and low concentrations of nitrogen monoxide (NO). As a potential explanation for the high OH concentrations, reformation of OH radicals from unimolecular reactions of organic peroxy radicals (RO<sub>2</sub>) that result from the reaction of isoprene with OH have been suggested (Peeters et al., 2009; Peeters and Müller, 2010; da Silva et al., 2010). 30 The proposed reactions involve 1,5-H- and 1,6-H-shift reactions followed by decomposition of specific isoprene RO<sub>2</sub> isomers and compete with the well-known OH reformation via reaction of HO<sub>2</sub> with NO. This reaction scheme has been applied, in order to explain high levels of OH radicals, using reaction rate constants that were derived from quantum chemical calculations (Taraborrelli et al., 2012). A laboratory study investigated the product yields of the proposed reactions (Crouse et al., 2011; Wolfe et al., 2012) and direct OH measurements in experiments in the atmosphere simulation chamber SAPHIR gave evidence for OH regeneration from isoprene RO<sub>2</sub> without involvement of NO (Fuchs et al., 2013). Results from these experimental studies are consistent with the RO<sub>2</sub> isomerization reaction scheme but also showed that isomerization reaction rate constants are smaller than originally calculated (Peeters and Müller, 2010). Thus, OH regeneration from isoprene peroxy radicals alone cannot explain elevated OH concentrations found in field campaigns. Therefore, the question arises, if unimolecular RO<sub>2</sub> reactions from the oxidation products of isoprene may also enhance atmospheric OH. 45

Methacrolein (2-methylpropanal) is one of the major first-generation products of the gas-phase oxidation of isoprene by OH with a yield of approximately 20–30 % for atmospheric conditions (Tuazon and Atkinson, 1990; Galloway et al., 2011). Methacrolein (MACR) is further oxidized by OH in the atmosphere producing hydroxyacetone, methylglyoxal, and formaldehyde (Galloway et al., 2011). Similar unimolecular reactions of RO<sub>2</sub> as for isoprene, which may produce additional OH, have also been suggested for MACR (Peeters et al., 2009; Crouse et al., 2012; Asatryan et al., 2010; da Silva, 2012). Recently, the product distribution from the MACR plus OH reaction for various NO concentrations has been investigated in a laboratory study accompanied by quantum 55



chemical calculations (Crouse et al., 2012). They inferred a new reaction pathway, in which hydroxyacetone is formed independently of the level of NO. This would be consistent with a fast unimolecular RO<sub>2</sub> reaction, because hydroxyacetone has so far only been known as a product of the reaction of RO<sub>2</sub> with NO. The new reaction path is attributed to a 1,4-H-shift isomerization reaction and implies reformation of OH -product (Crouse et al., 2012), but OH concentrations were not directly measured in that study.


Here, we present the investigation of the photo-oxidation of MACR by OH at controlled atmospheric conditions in the simulation chamber SAPHIR in the presence of approximately 90 pptv NO. Measurements of ~~all relevant trace gas concentrations, including~~ OH, hydroperoxy (HO<sub>2</sub>) and RO<sub>2</sub> radicals, and the OH lifetime allow a detailed analysis of the OH budget. Recently proposed reaction pathways are tested by comparing time series of measurements with model calculations.

## 2 Methods

### 2.1 Simulation experiment in SAPHIR

Experiments were conducted in the atmosphere simulation chamber SAPHIR in Jülich, Germany. The chamber allows to investigate the photochemical oxidation of organic compounds at atmospheric conditions with respect to temperature, pressure, radiation and concentrations of trace gases and radicals. Experiments for this study were similar to those that were performed to investigate the oxidation of isoprene by OH (Fuchs et al., 2013).

The outdoor SAPHIR chamber is made of a double wall Teflon (FEP) film of cylindrical shape (length 18 m, diameter 5 m, volume 270 m<sup>3</sup>). Details of the chamber have been described earlier (Rohrer et al., 2005; Bohn et al., 2005; Schlosser et al., 2009). It is equipped with a shutter system, which can be opened to expose the chamber air to natural sunlight. The FEP film has a high transmittance for the entire spectrum of solar radiation (Bohn et al., 2005). Slight overpressure prevents leakage of ambient air into the chamber. The chamber air is mixed from evaporated liquid nitrogen and oxygen of highest purity (Linde, purity > 99.99990 %). During all experiments reported here, a fan ensured fast mixing of the chamber air (mixing time < 2 min). Replenishment of chamber air, which is lost due to small leakages and consumption by instruments, leads to a dilution of trace gases with e of approximately 4 % h<sup>-1</sup>. .

The experiments aimed to simulate conditions like those found during field experiments (Lu et al., 2012, 2013), when unexpectedly large OH concentrations were measured. At the beginning of the experiment, the dark chamber only contained clean synthetic air. The water vapour mixing ratio was increased by flushing water vapour from boiling Milli-Q-water into the chamber in the dark, until the relative humidity reached approximately 80 %. n the shutter system was opened to expose the chamber to sunlight. Ozone produced from a silent discharge ozoniser was added resulting in a mixing ratio of approximately 50 ppbv. The initial phase (“ZA”) with zero air, water vapour, and

ozone had a total duration of 2 hours. Thereafter, MACR was injected several times increasing the mixing ratio by 7 ppbv each time. The maximum mixing ratio was 14 ppbv. The experiment was performed three times in a similar way (Table 1). On 11 August 2011 OH production rates from photolysis were highest and a large number of instruments was available. Therefore, time series and model calculations from this experiment are shown here. Experiments on the other two days give similar results and are included in the analysis of the OH budget.

The major primary source for OH in the chamber is photolysis of nitrous acid (HONO), which is released from the Teflon film depending on temperature, relative humidity, and strength of radiation (Rohrer et al., 2005). HONO photolysis is also the major source of nitrogen oxides. In addition, acetaldehyde and formaldehyde are formed with a rate of approximately  $200 \text{ pptv h}^{-1}$  during these experiments. The OH reactivity is on the order of  $(1-2) \text{ s}^{-1}$  in the absence of additional OH reactants, which can be partly explained by the presence of NO, NO<sub>2</sub>, formaldehyde (HCHO) and acetaldehyde (CH<sub>3</sub>CHO). RO<sub>2</sub> radicals of approximately  $(1-2) \times 10^8 \text{ cm}^{-3}$  were immediately formed in the humidified clean air when the chamber roof was opened. They were partly formed by photolytic processes. This is evident from reference experiments with CO, in which RO<sub>2</sub> radical concentrations persisted even though OH was completely scavenged by excess CO. Sources of trace gases and radicals can be well-parameterized from reference experiments, but except for the production of HONO they played only a minor role for the experiments after MACR had been injected.

## 2.2 Instrumentation

Trace gas and radical concentrations were measured by instruments listed in Table 2. A laser induced fluorescence instrument (LIF) was used to measure OH, HO<sub>2</sub>, and RO<sub>2</sub> concentrations simultaneously in three parallel measurement cells. RO<sub>2</sub> and HO<sub>2</sub> are detected via their conversion to OH involving reactions with NO. The signal of the HO<sub>2</sub> detection includes a small fraction of specific RO<sub>2</sub> species, which can be partly converted to OH on the same time-scale (Fuchs et al., 2011). Instrument parameters were optimized to minimize this interference. For RO<sub>2</sub>, the conversion efficiency is assumed to be small, if their conversion to OH requires more than two reactions with NO (like for acyl peroxy radicals), because of the short residence time between NO addition and OH detection in the instrument (Fuchs et al., 2008). The measured detection efficiency for MACR derived RO<sub>2</sub> which are efficiently converted is similar to that of methyl-peroxy radicals.

OH was also detected by a Differential Optical Absorption Spectrometer (DOAS) during two of the three experiments. As previously shown, measurements of both instruments (LIF and DOAS) agreed within their uncertainties during experiments in SAPHIR that were performed for the investigation of the oxidation of various organic compounds including MACR (Schlosser et al., 2007, 2009; Fuchs et al., 2012). This indicates that OH measurements were not affected by unknown interferences. During the experiment on 11 August 2011, the correlation between OH measurements by DOAS and LIF shows a small intercept of  $0.5 \times 10^6 \text{ cm}^{-3}$ , which was not observed in other exper-

iments investigating MACR oxidation (Fuchs et al., 2012). For the analysis of data from 11 August 2011 in Figs. 2 and 5, we chose the DOAS data, which is regarded to be an absolute measurement reference.

130 The chemical lifetime of OH was measured applying a combination of flash photolysis producing OH by ozone photolysis at 266 nm in a reaction cell under slow-flow conditions and time-resolved detection of OH by LIF. The evaluation of the pseudo-first order decays gives directly the rate coefficient of the OH loss (OH reactivity) or inverse OH lifetime. Organic compounds were measured by a Proton-Transfer-Reaction-Time-Of-Flight Mass-Spectrometry instrument (PTR-TOF-MS), nitro-  
135 gen oxides and ozone by chemiluminescence instruments and nitrous acid by a Long Path Absorption Photometer (LOPAP). During one of the experiments, peroxyacyl nitrates, PAN and MPAN, which serve as reservoirs for peroxy radicals and nitrogen oxides during MACR oxidation, were detected by gas chromatography (GC).

### 2.3 Model calculations

140 Time series of measurements were compared to calculations using the Master Chemical Mechanism version 3.2 (MCM) (Jenkin et al., 1997; Saunders et al., 2003) available at <http://mcm.leeds.ac.uk/MCM>. The MCM represents the current knowledge of atmospheric chemistry. In addition to the chemistry from the MCM, chamber specific properties were included in the model calculations. Dilution of trace gases due to the replenishment of zero air was modelled from monitored rates of the  
145 dilution flow. The dependence of source strengths for HONO, HCHO and CH<sub>3</sub>CHO on radiation, relative humidity and temperature were taken from parameterizations described earlier (Rohrer et al., 2005; Karl et al., 2006). The source strengths were scaled, in order to match formation of NO<sub>x</sub>, HCHO and CH<sub>3</sub>CHO during the zero air part of the experiment. The part of the OH reactivity (approximately 1 s<sup>-1</sup>) which could not be explained by the presence of measured OH reactants was  
150 treated as an OH reactant of constant concentration, which converts OH to HO<sub>2</sub> like CO does. The value of this “background” OH reactivity was determined from the measured OH reactivity at the start of the experiment (dark chamber), when only zero air and water vapour was present. Also RO<sub>2</sub> radicals were formed in the sunlit chamber from unknown sources. A photolytic RO<sub>2</sub> source was implemented in the model, which was similarly parameterized as the empirical functions for the  
155 HONO and HCHO sources. The applicability of this procedure was confirmed in test experiments, for which the production rate was scaled to match measured RO<sub>2</sub> concentrations.

The model was constrained by measurements of temperature, pressure, calculated dilution rates, measured water vapour mixing ratios, and photolysis frequencies for NO<sub>2</sub>, HCHO, O<sub>3</sub>, MACR and HONO. Photolysis frequencies and relative humidity constrained the calculated chamber sources for  
160 HONO, HCHO, and CH<sub>3</sub>CHO. Photolysis frequencies that were not measured were first calculated by a MCM (version 3.1) function for clear sky conditions and then scaled by the ratio of the measured and calculated NO<sub>2</sub> photolysis frequencies to account for reductions of the solar radiation by clouds

and the transmission of the Teflon film. Constrained parameters were re-initialized on a 1 min time grid. The injection of trace gases ( $O_3$ , MACR) was modelled as sources, which were turned on  
165 for the time of the injection. The source strength for ozone was adjusted to match the measured concentrations right after the injection and that for MACR was adjusted to match the change in the measured OH reactivity. Otherwise, trace gas concentrations were calculated by the model.

Modelled  $HO_2$  concentrations presented here are the sum of calculated  $HO_2$  and a fraction of specific  $RO_2$  that are an interference in the  $HO_2$  measurements (like introduced by Lu et al., 2012,  
170 as  $HO_2^*$ ), so that measurements can be compared to calculations. Model calculations taking  $RO_2$  conversion efficiency from characterization experiments of the instrument suggest that the contribution of this interference to the entire  $HO_2$  detection was less than 5 % for these experiments, most of which is caused by  $RO_2$  from MACR. Calculated  $RO_2$  concentrations that are shown in the following only include those  $RO_2$  species that are efficiently converted to OH in the  $RO_2$  measurement  
175 channel of the LIF instrument.

### 3 Results and discussion

#### 3.1 Time series of trace gas concentrations

Once the humidified clean air is exposed to sunlight, HONO is formed on the chamber walls. Its photolysis increases the concentrations of  $NO_x$  and OH (Fig. 1). During this initial phase of the  
180 experiment, the OH reactivity is only approximately  $1 s^{-1}$ , so that maximum OH concentrations of  $1 \times 10^7 cm^{-3}$  are reached (OH concentrations in Fig. 1 are scaled by a factor of 0.5 during this part of the experiment). MACR injections increase the OH reactivity to up to  $13.5 s^{-1}$ , so that OH concentrations drop to  $(1-1.5) \times 10^6 cm^{-3}$ . The maximum MACR mixing ratio after the last injection is 14 ppbv. OH dominantly reacts with MACR during the entire experiment (e.g.  
185 14 ppbv MACR corresponds to an OH reactivity of  $10 s^{-1}$ ). Reaction of OH with MACR initiates a reaction chain that produces  $RO_2$  and  $HO_2$ , which includes reactions with NO, so that  $RO_2$  and  $HO_2$  concentrations increase in the presence of MACR. Similarly, concentrations of radical reservoir species peroxyacetyl nitrate and peroxy methacryloyl nitrate, PAN and MPAN (Table 3), are increasing after each MACR injection. These species are products of the reaction of acyl peroxy  
190 radicals with  $NO_2$ . MPAN and PAN are thermally unstable (Roberts and Bertman, 1992), so that a thermal equilibrium is established. Because PAN is also formed from acetaldehyde in the sunlit chamber, the PAN mixing ratio starts increasing before MACR is injected. The NO concentration is nearly constant over the course of the experiment with a mixing ratio of approximately 90 pptv.

Model calculations applying MCM give OH concentrations, which are approximately 50 % lower  
195 than measurements during the MACR oxidation part of the experiment (Fig. 1). The increasing difference between measured and modelled MACR indicates that less MACR is oxidized in the model during the experiment supporting that OH concentrations in the chamber are indeed larger

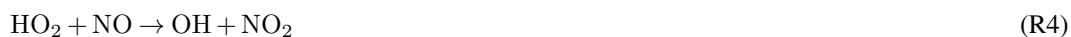
than calculated.

The reaction of OH with MACR produces three RO<sub>2</sub> species (MCM names: MACRO2, MACROHO2, 200 MACO3, Table 3). Measured RO<sub>2</sub> radical concentrations are reproduced by model calculations. Acyl peroxy radicals like MACO3 are detected by the LIF instrument with low sensitivity (see above). However, the good model-measurement agreement of MPAN and PAN mixing ratios, which are formed from MACO3, indicates that model calculations reproduce MACO3 concentrations. The shape of the temporal behavior of MPAN mixing ratios is determined by the thermal equilibrium between MPAN and MACO3, forcing the fast built up of MPAN after each methacrolein 205 injection. At later times, the MPAN reservoir starts to deplete, when MACO3 concentrations are decreasing with the decreasing production from the reaction of MACR with OH. HO<sub>2</sub> concentrations are slightly underestimated, but the difference is within the uncertainty of measurements (Table 2).

In general, the description of radical species by the MCM during the part of the experiment before 210 OH reactants are injected into the chamber is expected to be less accurate, because (1) the OH reactivity is mostly caused by unknown species and (2) radical sources and sinks are not well-defined. After the initial phase of the experiment the OH reactivity is dominated by MACR. Then, a much better model-measurement agreement can be expected, provided the underlying mechanism is correct, because chamber specific properties like the small OH reactivity from unknown species 215 do not any longer play a role. This has been shown in similar experiments, when CO or butene was the dominant OH reactant. model-measurement agreement for radical species within 30 % can be achieved in these reference experiments.

### 3.2 OH budget analysis

The significant underprediction of the measured OH concentration in the presence of MACR in the chamber experiments (Fig. 1) and the relative good agreement of the measured and modelled OH reactivity suggest a missing OH source in the model. The missing production rate can be analyzed by a model-independent approach by comparing the OH production and destruction rates of known processes (Hofzumahaus et al., 2009). Primary OH sources in the chamber are O<sub>3</sub> and HONO photolysis. Furthermore, OH is produced from radical recycling via the reaction of HO<sub>2</sub> with NO:



All three contributions to the entire OH production rate can be calculated using only experimental 220 data. Also the OH reactivity and the OH concentration were measured, so that the OH destruction rate can be calculated. Figure 2 shows time series of the OH production (summed up as coloured areas) and of the OH destruction rate for the experiment on 11 August 2011. Before MACR is

injected to the chamber air, the OH production is balanced by its destruction as expected for a short-lived species like OH under steady-state conditions. However, during the MACR oxidation part of the experiment the calculated OH destruction rate is on average twice as large as the sum of OH production from radical recycling via the HO<sub>2</sub> + NO reaction and O<sub>3</sub> and HONO photolysis. The grey shaded area in Fig. 2 indicates the additional OH production from an unknown source that is needed to balance the OH destruction (“missing OH source”). Apparently, the missing OH source is linked with the degradation of MACR by OH.

In the following, the data from all experiments are collectively analyzed to determine the missing OH source. This is justified because conditions of the experiments were similar (Table 1). The time-resolved missing OH source shows considerable variability over the course of all experiments, but no significant trend with time is seen in the data (Fig. 3, upper panel). This indicates that the additional OH is most likely not produced from longer-lived first-generation organic products of the MACR oxidation such as hydroxyacetone. These products would accumulate over the course of the experiment because they are less reactive towards OH (Butkovskaya et al., 2006). Therefore, an increasing OH production would be expected, if there was additional OH produced from these species.

Part of the variability of the time series of the missing OH production rate is caused by the variability of the production rate of RO<sub>2</sub> formed in the reaction of MACR with OH (Fig. 3). Here, the RO<sub>2</sub> production rate is calculated from measured OH and MACR concentrations assuming that every reaction of OH with MACR yields one RO<sub>2</sub> radical. Plotting the missing OH production rate against the RO<sub>2</sub> formation rate (Fig. 3) reveals a clear correlation between both values. This suggests that OH is formed from an RO<sub>2</sub> reaction channel missing in the MCM mechanism. The slope of the correlation would be the amount of OH that is additionally produced from each RO<sub>2</sub> radical. A weighted linear fit with a fixed zero offset gives a value of 0.77 ± 0.31. Here, the 1σ uncertainty of ±0.31 is determined by the 1σ accuracy of measurements that are included in both coordinates of the correlation (Fig. 3) giving an uncertainty of the slope of approximately ±0.31.

This additional reaction channel competes with the reaction of RO<sub>2</sub> with NO, which finally also regenerates OH, and the reaction of RO<sub>2</sub> with HO<sub>2</sub>, which is a radical termination reaction forming peroxides (ROOH):



The calculated yield of 0.77 ± 0.31 OH from RO<sub>2</sub> radical needed to close the OH budget can be regarded as the branching ratio of Reaction R7. The large value indicates that this reaction channel is an important pathway for conditions of these experiments (NO mixing ratios less than 100 pptv and HO<sub>2</sub> concentrations less than 6 × 10<sup>8</sup> cm<sup>-3</sup>).



### 3.3 Modifications of the MACR oxidation scheme

#### 3.3.1 Generic OH recycling with X

A large discrepancy between measured and modelled OH concentrations has been observed in several field campaigns. In order to explain the high OH concentrations in some field campaigns, a generic recycling of OH radicals by a constant amount of an unknown compound X was assumed that would convert peroxy radicals to OH like NO does, but without accompanying ozone production (Hofzumahaus et al., 2009; Lu et al., 2012, 2013):



255 Different amounts of X (in units of NO equivalents) were required: Pearl-River-Delta 800 pptv  
(Hofzumahaus et al., 2009; Lu et al., 2012), Beijing 400 pptv (Lu et al., 2013), and Borneo 700 pptv  
(Whalley et al., 2011). The nature of X, however, remained unclear, so that this mechanism could  
only serve as an empirical description. Recently, generic OH recycling was also applied, in order  
to describe fast OH regeneration from isoprene oxidation by OH in experiments in the SAPHIR  
260 chamber (Fuchs et al., 2013). A constant NO equivalent of 100 pptv was required in this case. It  
was shown that the effect of a generic OH recycling by X had the same effect as OH production  
from RO<sub>2</sub> radical isomerization and decomposition reactions.

Generic OH recycling by X is also tested for MACR oxidation experiments here, in order to  
see, if this empirical mechanism can also describe observations like shown for isoprene oxidation  
265 experiments. In fact, all observations including those of OH and MACR can be reproduced, if the  
mixing ratio of X is assumed to be equivalent to 50 pptv NO (Figs. 4 and 5). This amount of X is  
only half of what was found for isoprene oxidation for similar conditions (Fuchs et al., 2013) and is  
approximately ten times smaller compared to the amount of X that was needed to explain the above  
mentioned field observations.

#### 270 3.3.2 RO<sub>2</sub> isomerization reactions.

The reaction of OH with MACR either leads to OH addition to the C=C double bond or H-  
abstraction from the CHO group (Tuazon and Atkinson, 1990; Orlando et al., 1999). OH adds  
dominantly to the external olefinic carbon atom (yield MCM: 47 %, Fig. 6) forming an RO<sub>2</sub> radical  
after reaction with O<sub>2</sub> (MCM: MACRO2). OH addition to the internal carbon atom is less likely  
275 (yield MCM: 8 %) and forms a different RO<sub>2</sub> radical after reaction with O<sub>2</sub> (MCM: MACROHO2).  
H-abstraction from the CHO group of MACR leads to the formation of an acyl peroxy radical after  
reaction with O<sub>2</sub> (MCM: MACO3, yield 45 %, Fig. 6).

Recent work has shown that the yield of OH from the reaction of HO<sub>2</sub> with acyl peroxy radicals  
like MACO3 could be larger than thought before (Dillon and Crowley, 2008; Taraborrelli et al.,

280 2012). The chemical model MCM used in this work assumes an OH yield of 0.44 for the reac-  
tion of HO<sub>2</sub> with MACO<sub>3</sub>, whereas a yield of <0.7 was found for the simplest acyl peroxy radical  
CH<sub>3</sub>CO<sub>3</sub> (Dillon and Crowley, 2008; Groß, 2014). Although the qualitative behaviour of the miss-  
ing OH source would be consistent with a larger OH yield from the reaction of HO<sub>2</sub> with MACO<sub>3</sub>  
(Fig. 3), the turnover rate of this reaction is too small, in order to significantly increase the OH  
285 production rate. Doubling of the OH yield would increase the OH production rate by less than  
0.1 ppbv h<sup>-1</sup>, much smaller than the missing OH production rate.

Quantum chemical calculations showed that RO<sub>2</sub> isomerization with subsequent decomposition  
could lead to a fast OH regeneration from RO<sub>2</sub> from isoprene via 1,5-H-shift or 1,6-H-shift iso-  
merization with subsequent decomposition of the products (Peeters et al., 2009; Peeters and Müller,  
290 2010; da Silva et al., 2010). Similar reaction schemes have also been proposed for MACR (Peeters  
et al., 2009; Crouse et al., 2012; Asatryan et al., 2010; da Silva, 2012). A 1,5-H-shift for MACRO<sub>2</sub>  
with subsequent decomposition would produce methylglyoxal, formaldehyde and OH, ~~but an only  
small reaction-rate~~ constant of less than 0.008 s<sup>-1</sup> at 303 K has been calculated (Peeters et al., 2009;  
Crouse et al., 2012). Because additional OH from this isomerization reaction applies only for one  
295 RO<sub>2</sub> isomer (MACRO<sub>2</sub>) from the OH + MACR reaction and the rate constant is relatively small,  
the amount of additional OH from this isomerization channel is rather small. Time series of mod-  
elled radical and trace gas concentrations are shown in Fig. 4 for this case and Fig. 5 displays the  
ratio of measured to modelled OH concentrations. The 1,5-H-shift ~~alone~~ only slightly improves the  
model-measurement agreement.

300 In addition to the 1,5-H-shift of MACRO<sub>2</sub>, a much faster 1,4-H-shift for MACRO<sub>2</sub> and a fast  
1,5-H-shift for MACROHO<sub>2</sub> with an isomerization rate constant of (0.5 ± 0.3) s<sup>-1</sup> at 296 K for  
both reactions have been suggested (Crouse et al., 2012). The 1,5-H-shift of the aldehyde H-atom  
in MACROHO<sub>2</sub> would produce hydroperoxyacetone (MCM: HYPERACET, Table 3), CO and  
HO<sub>2</sub>. The 1,4-H-shift of MACRO<sub>2</sub> would lead to the formation of hydroxyacetone, CO and OH  
305 (Crouse et al., 2012) (Fig. 6). A laboratory study (Crouse et al., 2012) shows that hydroxyacetone  
concentrations, which were measured in MACR oxidation experiments with low NO concentra-  
tions, are much larger than expected. According to the study by Crouse et al. (2012) this result  
is consistent with the fast production of hydroxyacetone in the 1,4-H-shift isomerization channel  
of MACRO<sub>2</sub>. Application of a temperature dependence as suggested in literature (Crouse et al.,  
310 2012) yields a rate constant of 0.66 s<sup>-1</sup> at the temperature during the experiment on 11 August 2011  
(301 K). For conditions of this experiment, more than 95 % of the MACRO<sub>2</sub> would undergo the  
1,4-H-shift. Also the branching ratio of the 1,5-H-shift for MACROHO<sub>2</sub> would be 95 %, if the  
reaction rate constant was similarly large as suggested. Figure 4 shows time series of concentrations  
and Fig. 5 the ratio of measured to modelled OH concentrations (case B), if both, the 1,4-H-shift  
315 of MACRO<sub>2</sub> and the 1,5-H-shift of MACROHO<sub>2</sub>, are included. All observations, especially OH  
concentrations, are matched in this case. Most of the additional OH is formed by the 1,4-H-shift

reaction of MACRO2. At the end of the experiment, the isomerization mechanism is expected to increase the hydroxyacetone mixing ratio by 1.5 ppbv compared to MCM calculations (Fig. 4).

~~Sensitivity~~ model calculations with variation of the 1,4-H-shift isomerization rate constant were performed to estimate the sensitivity of calculated OH concentrations for experiments here. Decreasing the isomerization rate to a value, for which the median of the difference between measured and modelled OH has a maximum value of 30 % (the agreement that is expected from reference experiments), gives a lower limit of the rate constant constant of  $0.03 \text{ s}^{-1}$ , ~~for which model calculations would be still consistent with the observations.~~ In this case, the MACRO2 isomerization reaction would regenerate 50 % of the OH radicals that were consumed in the MACR+OH reaction to produce MACRO2. This result is independent of the choice of OH data from either the DOAS or the LIF instrument, because the lower limit is determined by the slightly smaller OH concentrations measured by DOAS compared to LIF (see above). In contrast, modelled OH concentrations are insensitive to a reaction rate constant larger than suggested in literature (Crouse et al., 2012). In this case, MACRO2 and also MACROHO2 radicals nearly exclusively undergo isomerization for conditions of this experiment (Fig. 6). The yield of OH regenerated by isomerization becomes limited by the yields of MACRO2 and MACROHO2 from the reaction of MACR with OH. Our OH yield of 0.77 for each OH radical consumed by MACR (Fig. 3) is larger than the yield of 0.55 predicted by the model calculation, if MACRO2 and MACROHO2 is completely converted to OH in the isomerization reaction. This is, however, no contradiction considering the relative large uncertainty of  $\pm 0.3$  ( $1\sigma$ ) of our experimental value and the uncertainty of the model. Thus, our SAPHIR experiments presented in this work do not allow to determine an upper limit of the 1,4-H-shift isomerization rate constant.


Besides thermal decomposition of  $\text{RO}_2$  another reaction scheme has been proposed from quantum-chemical calculations (da Silva, 2012; Asatryan et al., 2010). This suggests that the vibrationally excited adduct of MACR and OH reacts with  $\text{O}_2$  on a similar time-scale as collisional deactivation of the adduct takes place. As a consequence, approximately 20 % of the MACR-OH adduct would react with  $\text{O}_2$  and would form “double activated”  $\text{RO}_2$  radicals, which then can decompose (da Silva, 2012). Decomposition of the “double activated”  $\text{RO}_2$  would lead to the formation of either methylglyoxal, formaldehyde and OH or hydroxyacetone, CO and OH. In the result, this mechanism is equivalent to the 1,4- and 1,5-H-shift isomerization reactions (Table 4) and would be equivalent to a maximum isomerization rate constant of  $0.007 \text{ s}^{-1}$ , in order to yield a branching ratio of maximum 20 % for conditions of these experiments. As shown above, more than 50 % of MACRO2 needs to immediately regenerate OH, in order to explain our observations, much larger than the 20 % yield of “double activated”  $\text{RO}_2$ . Therefore, this mechanism alone is not sufficient to bring calculations and measurements into agreement. Nevertheless, part of the discrepancy could be potentially due to the decomposition of “double-activated”  $\text{RO}_2$ , because it is not possible to distinguish both mechanisms in our experiments.

The 1,4-H-shift isomerization rate constant that is required to explain observations from MACRO2  
355 isomerization ( $> 0.03 \text{ s}^{-1}$ ) is equivalent to the reaction of MACRO2 with more than 150 pptv NO.  
This value is larger than the amount of X that is needed to describe measured OH concentrations  
in the “X”-mechanism (see above). In the “X”-mechanism 50 pptv X is equivalent to an additional  
RO<sub>2</sub> loss rate of  $0.01 \text{ s}^{-1}$ . However, in the “X”-mechanism, additional OH is recycled by all RO<sub>2</sub>  
360 species, so that the overall impact is larger than that from MACRO2 alone. Therefore, the 1,4-H-  
shift isomerization rate constant cannot be directly compared to the loss rate of MACRO2 with X  
in the “X”-mechanism.

#### 4 Summary and conclusions

Measured OH concentrations during MACR oxidation experiments in the atmosphere simulation  
chamber SAPHIR are underestimated by ~~chemical models~~ by approximately 50 % (NO mixing ratios  
365 approximately 90 pptv, HO<sub>2</sub> concentrations approximately  $5 \times 10^8 \text{ cm}^{-3}$  and  $T = 301 \text{ K}$ ). The  
analysis of the OH budget reveals that an additional OH source is required to balance the measured  
OH destruction rate. ~~Experiments allow to constrain the overall strength of the OH source regardless  
of the exact chemical mechanism that is responsible for the OH production.~~

~~Potential mechanisms behind the missing OH source can be the~~ production of OH from uni-  
370 molecular isomerization and decomposition reactions of RO<sub>2</sub> radicals (Peeters et al., 2009; Crouse  
et al., 2012; Asatryan et al., 2010; da Silva, 2012) and the decomposition of double activated RO<sub>2</sub>  
(Asatryan et al., 2010; da Silva, 2012) ~~both giving the same products. All mechanisms would en-  
hance OH by producing~~ OH from RO<sub>2</sub> without reactions with NO, consistent with observations  
here. However, only the 1,4-H-shift (Crouse et al., 2012) ~~would be strong~~ enough to bring ob-  
375 servations and calculations into agreement, whereas the 1,5-H-shift and decomposition of double  
activated RO<sub>2</sub> ~~would~~ only slightly improve the agreement between model calculations and measure-  
ments. Model calculations are consistent with the observations within the expected agreement, if  
the reaction rate constant for the 1,4-H-shift of the RO<sub>2</sub> isomer MACRO2 is ~~larger~~ than  $0.03 \text{ s}^{-1}$ .  
In this case, at least 50 % of MACRO2 undergoes the 1,4-H-shift reaction instead of reacting with  
380 NO or HO<sub>2</sub> as assumed in ~~chemical models like~~ the MCM. Thus, the 1,4-H-shift reaction ~~would be~~  
competitive to the reaction of MACRO2 with 150 pptv NO or even higher NO mixing ratios.

A yield of  $0.77 \pm 0.31$  for additionally produced OH is found from the OH budget analysis in these  
experiments. ~~It is maximum 0.55, if unimolecular RO<sub>2</sub> reactions of MACRO2 and MACROHO2  
are responsible for the additional OH~~ as suggested by Crouse et al. (2012). This value is compa-  
385 rable to the overall yield of OH from  unimolecular RO<sub>2</sub> reactions produced from isoprene-derived  
RO<sub>2</sub> (38–45 %) for similar conditions (Fuchs et al., 2013). However, the impact of these reaction  
pathways is less for MACR compared to isoprene for two reasons: (1) typical MACR mixing ratios  
are smaller compared to isoprene, because MACR is a product of isoprene degradation with a yield



of less than 30 % (Galloway et al., 2011) and (2) its reaction rate constant with OH is 3.5 times  
390 smaller, so that the MACR oxidation rate and therefore the production rate of MACR derived RO<sub>2</sub>  
is smaller.

During field campaigns in the Amazonian rainforest, when unexpected large OH was found, isoprene was the dominant OH reactant. Measurements of the sum of MVK and MACR also indicate substantial amounts of MACR (Kubistin et al., 2010). Assuming that at most half of the measured  
395 MVK + MACR concentration was MACR, MACR mixing ratios were only 20 % of the mixing ratio of isoprene, when the largest discrepancy between measured and predicted OH was found (Kubistin et al., 2010). ~~Taking also~~ the smaller reaction rate constant of MACR with OH ~~into account~~, the contribution of additional OH from MACR oxidation was significant, but most likely much smaller compared to that from isoprene. Because additional OH production from isoprene alone  
400 can only explain a smaller part of the entire gap between measured and predicted OH (Fuchs et al., 2013), the contribution of additional OH from MACR derived RO<sub>2</sub> is most likely not large enough to close the remaining gap. During field measurements in China, MACR oxidation played only a minor role (Lou et al., 2010), so that the impact of additional OH recycling from MACR-derived RO<sub>2</sub> is rather small. Nevertheless, results here show that the class of RO<sub>2</sub> isomerization reactions  
405 plays an important role at atmospheric conditions with low NO concentrations.

*Acknowledgements.* This work was supported by the EU FP-7 program EUROCHAMP-2 (grant agreement no. 228335) and by the EU FP-7 program PEGASOS (grant agreement no. 265307). S. Nehr and B. Bohn thank the Deutsche Forschungsgemeinschaft for funding (grant BO 1580/3-1). The authors thank A. Buchholz, P. Schlag, F. Rubach, H.-C. Wu, S. Dixneuf, M. Vietz, P. Müsgen, and M. Bachner for additional measurements  
410 during this campaign and technical support. The authors also thank G. da Silva for helpful discussions.

The service charges for this open access publication have been covered by a Research Centre of the Helmholtz Association.

## References

- 415 Asatryan, R., da Silva, G., and Bozelli, J. W.: Quantum chemical study of the acrolein ( $\text{CH}_2\text{CHCHO}$ ) + OH +  $\text{O}_2$  reactions, *J. Phys. Chem. A*, 114, 8302–8311, doi:10.1021/jp104828a, 2010.
- Bohn, B., Rohrer, F., Brauers, T., and Wahner, A.: Actinometric measurements of  $\text{NO}_2$  photolysis frequencies in the atmosphere simulation chamber SAPHIR, *Atmos. Chem. Phys.*, 5, 493–503, doi:10.5194/acp-5-493-2005, 2005.
- 420 Butkovskaya, N. I., Pouvesle, N., Kukui, A., Mu, Y., and Le Bras, G.: Mechanism of the OH-initiated oxidation of hydroxyacetone over the temperature range 236–298 K, *J. Phys. Chem. A*, 110, 6833–6843, doi:10.1021/jp056345r, 2006.
- Carslaw, N., Creasey, D. J., Harrison, D., Heard, D. E., Hunter, M. C., Jacobs, P. J., Jenkin, M. E., Lee, J. D., Lewis, A. C., Pilling, M. J., Saunders, S. M., and Seakins, P. W.: OH and  $\text{HO}_2$  radical chemistry in a forested  
425 region of north-western Greece, *Atmos. Environ.*, 35, 4725–4737, doi:10.1016/s1352-2310(01)00089-9, 2001.
- Crounse, J. D., Paulot, F., Kjaergaard, H. G., and Wennberg, P. O.: Peroxy radical isomerization in the oxidation of isoprene, *Phys. Chem. Chem. Phys.*, 13, 13607–13613, doi:10.1039/C1CP21330J, 2011.
- Crounse, J. D., Knap, H. C., Ornsø, K. B., Jørgensen, S., Paulot, F., Kjaergaard, H. G., and Wennberg, P. O.: On  
430 the atmospheric fate of methacrolein: 1. Peroxy radical isomerization following addition of OH and  $\text{O}_2$ , *J. Phys. Chem. A*, 116, 5756–5762, doi:10.1021/jp211560u, 2012.
- da Silva, G.: Reaction of methacrolein with the hydroxyl radical in air: incorporation of secondary  $\text{O}_2$  addition into the MACR + OH master equation, *J. Phys. Chem. A*, 116, 5317–5324, doi:10.1021/jp303806w, 2012.
- da Silva, G., Graham, C., and Wang, Z.-F.: Unimolecular  $\beta$ -hydroxyperoxy radical decomposition  
435 with OH recycling in the photochemical oxidation of isoprene, *Environ. Sci. Technol.*, 44, 250–256, doi:10.1021/es900924d, 2010.
- Dillon, T. J. and Crowley, J. N.: Direct detection of OH formation in the reactions of  $\text{HO}_2$  with  $\text{CH}_3\text{C}(\text{O})\text{O}_2$  and other substituted peroxy radicals, *Atmos. Chem. Phys.*, 8, 4877–4889, doi:10.5194/acp-8-4877-2008, 2008.
- 440 Dorn, H.-P., Brandenburger, U., Brauers, T., and Hausmann, M.: A new in-situ laser long-path absorption instrument for the measurement of tropospheric OH radicals, *J. Atmos. Sci.*, 52, 3373–3380, 1995.
- Fuchs, H., Hofzumahaus, A., and Holland, F.: Measurement of tropospheric  $\text{RO}_2$  and  $\text{HO}_2$  radicals by a laser-induced fluorescence instrument, *Rev. Sci. Instrum.*, 79, 084104, doi:10.1063/1.2968712, 2008.
- Fuchs, H., Bohn, B., Hofzumahaus, A., Holland, F., Lu, K. D., Nehr, S., Rohrer, F., and Wahner, A.: Detection  
445 of  $\text{HO}_2$  by laser-induced fluorescence: calibration and interferences from  $\text{RO}_2$  radicals, *Atmos. Meas. Tech.*, 4, 1209–1225, doi:10.5194/amt-4-1209-2011, 2011.
- Fuchs, H., Dorn, H.-P., Bachner, M., Bohn, B., Brauers, T., Gomm, S., Hofzumahaus, A., Holland, F., Nehr, S., Rohrer, F., Tillmann, R., and Wahner, A.: Comparison of OH concentration measurements by DOAS and LIF during SAPHIR chamber experiments at high OH reactivity and low NO concentration, *Atmos. Meas.*  
450 *Tech.*, 5, 1611–1626, doi:10.5194/amt-5-1611-2012, 2012.
- Fuchs, H., Hofzumahaus, A., Rohrer, F., Bohn, B., Brauers, T., Dorn, H.-P., Häsel, R., Holland, F., Kaminski, M., Li, X., Lu, K., Nehr, S., Tillmann, R., Wegener, R., and Wahner, A.: Experimental evidence for efficient hydroxyl radical regeneration in isoprene oxidation, *Nat. Geosci.*, 6, 1023–1026,

- doi:10.1038/NGEO1964, 2013.
- 455 Galloway, M. M., Huisman, A. J., Yee, L. D., Chan, A. W. H., Loza, C. L., Seinfeld, J. H., and Keutsch, F. N.: Yields of oxidized volatile organic compounds during the OH radical initiated oxidation of isoprene, methyl vinyl ketone, and methacrolein under high-NO<sub>x</sub> conditions, *Atmos. Chem. Phys.*, 11, 10779–10790, doi:10.5194/acp-11-10779-2011, 2011.
- Groß, C. B. M., Dillon, T. J., Schuster, G., Lelieveld, J., and Crowley, J. N.: Direct kinetic study of  
460 OH and O<sub>3</sub> formation in the reaction of CH<sub>3</sub>C(O)O<sub>2</sub> with HO<sub>2</sub>, *J. Phys. Chem. A*, 118, 974–985, doi:10.1021/jp412380z, 2014.
- Guenther, A. B., Jiang, X., Heald, C. L., Sakulyanontvittaya, T., Duhl, T., Emmons, L. K., and Wang, X.: The Model of Emissions of Gases and Aerosols from Nature version 2.1 (MEGAN2.1): an extended and updated framework for modeling biogenic emissions, *Geosci. Model Dev.*, 5, 1471–1492, doi:10.5194/gmd-5-1471-  
465 2012, 2012.
- Häseler, R., Brauers, T., Holland, F., and Wahner, A.: Development and application of a new mobile LOPAP instrument for the measurement of HONO altitude profiles in the planetary boundary layer, *Atmos. Meas. Tech. Discuss.*, 2, 2027–2054, doi:10.5194/amtd-2-2027-2009, 2009.
- Hausmann, M., Brandenburger, U., Brauers, T., and Dorn, H.-P.: Detection of tropospheric OH radicals by long-  
470 path differential-optical-absorption spectroscopy: Experimental setup, accuracy, and precision, *J. Geophys. Res.*, 102, 16011–16022, doi:10.1029/97jd00931, 1997.
- Hofzumahaus, A., Rohrer, F., Lu, K., Bohn, B., Brauers, T., Chang, C.-C., Fuchs, H., Holland, F., Kita, K., Kondo, Y., Li, X., Lou, S., Shao, M., Zeng, L., Wahner, A., and Zhang, Y.: Amplified trace gas removal in the troposphere, *Science*, 324, 1702–1704, doi:10.1126/science.1164566, 2009.
- 475 Jenkin, M. E., Saunders, S. M., and Pilling, M. J.: The tropospheric degradation of volatile organic compounds: a protocol for mechanism development, *Atmos. Environ.*, 31, 81–104, 1997.
- Jordan, A., Haidacher, S., Hanel, G., Hartungen, E., Märk, L., Seehauser, H., Schottkowsky, R., Sulzer, P., and Märk, T. D.: A high resolution and high sensitivity proton-transfer-reaction time-of-flight mass spectrometer (PTR-TOF-MS), *Int. J. Mass Spectrom.*, 286, 122–128, doi:10.1016/j.ijms.2009.07.005, 2009.
- 480 Karl, M., Dorn, H. P., Holland, F., Koppmann, R., Poppe, D., Rupp, L., Schaub, A., and Wahner, A.: Product study of the reaction of OH radicals with isoprene in the atmosphere simulation chamber SAPHIR, *J. Atmos. Chem.*, 55, 167–187, doi:10.1007/s10874-006-9034-x, 2006.
- Kelly, T. J. and Fortune, C. R.: Continuous monitoring of gaseous formaldehyde using an improved fluorescence approach, *Int. J. Anal. Chem.*, 54, 249–263, 1994.
- 485 Kubistin, D., Harder, H., Martinez, M., Rudolf, M., Sander, R., Bozem, H., Eerdeken, G., Fischer, H., Gurk, C., Klüpfel, T., Königstedt, R., Parchatka, U., Schiller, C. L., Stickler, A., Taraborrelli, D., Williams, J., and Lelieveld, J.: Hydroxyl radicals in the tropical troposphere over the Suriname rainforest: comparison of measurements with the box model MECCA, *Atmos. Chem. Phys.*, 10, 9705–9728, doi:10.5194/acp-10-9705-2010, 2010.
- 490 Kuhn, U., Andreae, M. O., Ammann, C., Araújo, A. C., Brancaleoni, E., Ciccioli, P., Dindorf, T., Frattoni, M., Gatti, L. V., Ganzeveld, L., Kruijt, B., Lelieveld, J., Lloyd, J., Meixner, F. X., Nobre, A. D., Pöschl, U., Spirig, C., Stefani, P., Thielmann, A., Valentini, R., and Kesselmeier, J.: Isoprene and monoterpene fluxes from Central Amazonian rainforest inferred from tower-based and airborne measurements, and implica-



- tions on the atmospheric chemistry and the local carbon budget, *Atmos. Chem. Phys.*, 7, 2855–2879, doi:10.5194/acp-7-2855-2007, 2007.
- 495 Lelieveld, J., Butler, T. M., Crowley, J. N., Dillon, T. J., Fischer, H., Ganzeveld, L., Harder, H., Lawrence, M. G., Martinez, M., Taraborrelli, D., and Williams, J.: Atmospheric oxidation capacity sustained by a tropical forest, *Nature*, 452, 737–740, doi:10.1038/nature06870, 2008.
- Lindinger, W., Hansel, A., and Jordan, A.: On-line monitoring of volatile organic compounds at pptv levels  
500 by means of proton-transfer-reaction mass spectrometry (PTR-MS) – Medical applications, food control and environmental research, *Int. J. Mass Spectrom.*, 173, 191–241, doi:10.1016/s0168-1176(97)00281-4, 1998.
- Lou, S., Holland, F., Rohrer, F., Lu, K., Bohn, B., Brauers, T., Chang, C.C., Fuchs, H., Häseler, R., Kita, K., Kondo, Y., Li, X., Shao, M., Zeng, L., Wahner, A., Zhang, Y., Wang, W., and Hofzumahaus, A.: Atmospheric OH reactivities in the Pearl River Delta – China in summer 2006: measurement and model results, *Atmos. Chem. Phys.*, 10, 11243–11260, doi:10.5194/acp-10-11243-2010, 2010.
- 505 Lu, K. D., Rohrer, F., Holland, F., Fuchs, H., Bohn, B., Brauers, T., Chang, C. C., Häseler, R., Hu, M., Kita, K., Kondo, Y., Li, X., Lou, S. R., Nehr, S., Shao, M., Zeng, L. M., Wahner, A., Zhang, Y. H., and Hofzumahaus, A.: Observation and modelling of OH and HO<sub>2</sub> concentrations in the Pearl River Delta 2006: a missing OH source in a VOC rich atmosphere, *Atmos. Chem. Phys.*, 12, 1541–1569, doi:10.5194/acp-12-1541-2012, 2012.
- 510 Lu, K. D., Hofzumahaus, A., Holland, F., Bohn, B., Brauers, T., Fuchs, H., Hu, M., Häseler, R., Kita, K., Kondo, Y., Li, X., Lou, S. R., Oebel, A., Shao, M., Zeng, L. M., Wahner, A., Zhu, T., Zhang, Y. H., and Rohrer, F.: Missing OH source in a suburban environment near Beijing: observed and modelled OH and HO<sub>2</sub> concentrations in summer 2006, *Atmos. Chem. Phys.*, 13, 1057–1080, doi:10.5194/acp-13-1057-2013, 2013.
- 515 Orlando, J. J., Tyndall, G. S., Fracheboud, J.-M., Estupiñan, E. G., Haberkorn, S., and Zimmer, A.: The rate and mechanism of the gas-phase oxidation of hydroxyacetone, *Atmos. Environ.*, 33, 1621–1629, doi:10.1016/s1352-2310(98)00386-0, 1999.
- Peeters, J. and Müller, J.-F.: HO<sub>x</sub> radical regeneration in isoprene oxidation via peroxy radical isomerisations, 2: experimental evidence and global impact, *Phys. Chem. Chem. Phys.*, 12, 14227–14235, doi:10.1039/C0CP00811G, 2010.
- 520 Peeters, J., Nguyen, T. L., and Vereecken, L.: HO<sub>x</sub> radical regeneration in the oxidation of isoprene, *Phys. Chem. Chem. Phys.*, 11, 5935–5939, doi:10.1039/b908511d, 2009.
- Ren, X., Olson, J. R., Crawford, J. H., Brune, W. H., Mao, J., Long, R. B., Chen, Z., Chen, G., Avery, M. A., Sachse, G. W., Barrick, J. D., Diskin, G. S., Huey, L. G., Fried, A., Cohen, R. C., Heikes, B., Wennberg, P. O., Singh, H. B., Blake, D. R., and Shetter, R. E.: HO<sub>x</sub> chemistry during INTEX-A 2004: observation, model calculation, and comparison with previous studies, *J. Geophys. Res.*, 113, D05310, doi:10.1029/2007JD009166, 2008.
- 525 Ridley, B. A., Grahek, F. E., and Walega, J. G.: A small, high-sensitivity, medium-response ozone detector suitable for measurements from light aircraft, *J. Atmos. Ocean. Tech.*, 9, 142–148, doi:10.1175/1520-0426(1992)009<0142:ASHSMR>2.0.CO;2, 1992.
- 530 Roberts, J. M. and Bertman, S. B.: The thermal decomposition of peroxyacetic nitric anhydride (PAN) and peroxyacrylic nitric anhydride (MPAN), *Int. J. Chem. Kin.*, 24, 297–307, doi:10.1002/kin.550240307,

- 1992.
- 535 Rohrer, F. and Brüning, D.: Surface NO and NO<sub>2</sub> mixing ratios measured between 30° N and 30° S in the Atlantic region, *J. Atmos. Chem.*, 15, 253–267, 1992.
- Rohrer, F., Bohn, B., Brauers, T., Brüning, D., Johnen, F.-J., Wahner, A., and Kleffmann, J.: Characterisation of the photolytic HONO-source in the atmosphere simulation chamber SAPHIR, *Atmos. Chem. Phys.*, 5, 2189–2201, doi:10.5194/acp-5-2189-2005, 2005.
- 540 Saunders, S. M., Jenkin, M. E., Derwent, R. G., and Pilling, M. J.: Protocol for the development of the Master Chemical Mechanism, MCM v3 (Part A): tropospheric degradation of non-aromatic volatile organic compounds, *Atmos. Chem. Phys.*, 3, 161–180, doi:10.5194/acp-3-161-2003, 2003.
- Schlosser, E., Bohn, B., Brauers, T., Dorn, H.-P., Fuchs, H., Häsel, R., Hofzumahaus, A., Holland, F., Rohrer, F., Rupp, L. O., Siese, M., Tillmann, R., and Wahner, A.: Intercomparison of two hydroxyl radical measurement techniques at the atmosphere simulation chamber SAPHIR, *J. Atmos. Chem.*, 56, 187–205, doi:10.1007/s10874-006-9049-3, 2007.
- 545 Schlosser, E., Brauers, T., Dorn, H.-P., Fuchs, H., Häsel, R., Hofzumahaus, A., Holland, F., Wahner, A., Kanaya, Y., Kajii, Y., Miyamoto, K., Nishida, S., Watanabe, K., Yoshino, A., Kubistin, D., Martinez, M., Rudolf, M., Harder, H., Berresheim, H., Elste, T., Plass-Dülmer, C., Stange, G., and Schurath, U.: Technical Note: Formal blind intercomparison of OH measurements: results from the international campaign HOxComp, *Atmos. Chem. Phys.*, 9, 7923–7948, doi:10.5194/acp-9-7923-2009, 2009.
- 550 Stone, D., Evans, M. J., Commane, R., Ingham, T., Floquet, C. F. A., McQuaid, J. B., Brookes, D. M., Monks, P. S., Purvis, R., Hamilton, J. F., Hopkins, J., Lee, J., Lewis, A. C., Stewart, D., Murphy, J. G., Mills, G., Oram, D., Reeves, C. E., and Heard, D. E.: HO<sub>x</sub> observations over West Africa during AMMA: impact of isoprene and NO<sub>x</sub>, *Atmos. Chem. Phys.*, 10, 9415–9429, doi:10.5194/acp-10-9415-2010, 2010.
- 555 Tan, D., Faloon, I., Simpas, J. B., Brune, W., Shepson, P. B., Couch, T. L., Summer, A. L., Carroll, M. A., Thornberry, T., Apel, E., Riemer, D., and Stockwell, W.: HO<sub>x</sub> budget in a deciduous forest: results from the PROPHET summer 1998 campaign, *J. Geophys. Res.*, 106, 24407–24427, 2001.
- Taraborrelli, D., Lawrence, M. G., Crowley, J. N., Dillon, T. J., Gromov, S., Grosz, C. B. M., Vereecken, L., and 560 Lelieveld, J.: Hydroxyl radical buffered by isoprene oxidation over tropical forests, *Nat. Geosci.*, 5, 190–193, doi:10.1038/ngeo1405, 2012.
- Tuazon, E. C. and Atkinson, R.: A product study of the gas-phase reaction of methacrolein with the OH radical in the presence of NO<sub>x</sub>, *Int. J. Chem. Kin.*, 22, 591–602, doi:10.1002/kin.550220604, 1990.
- Volz-Thomas, A., Xueref, I., and Schmitt, R.: An automatic gas chromatograph and calibration system for 565 ambient measurements of PAN and PPN, *Environ. Sci. Pollut. Res.*, 4, 72–76, 2002.
- Whalley, L. K., Edwards, P. M., Furneaux, K. L., Goddard, A., Ingham, T., Evans, M. J., Stone, D., Hopkins, J. R., Jones, C. E., Karunaharan, A., Lee, J. D., Lewis, A. C., Monks, P. S., Moller, S. J., and Heard, D. E.: Quantifying the magnitude of a missing hydroxyl radical source in a tropical rainforest, *Atmos. Chem. Phys.*, 11, 7223–7233, doi:10.5194/acp-11-7223-2011, 2011.
- 570 Wolfe, G. M., Thornton, J. A., Bouvier-Brown, N. C., Goldstein, A. H., Park, J.-H., McKay, M., Matross, D. M., Mao, J., Brune, W. H., LaFranchi, B. W., Browne, E. C., Min, K.-E., Wooldridge, P. J., Cohen, R. C., Crouse, J. D., Faloon, I. C., Gilman, J. B., Kuster, W. C., de Gouw, J. A., Huisman, A., and Keutsch, F. N.: The Chemistry of Atmosphere-Forest Exchange (CAFE) Model – Part 2: Application to BEARPEX-2007

**Table 1.** Experimental conditions of the MACR oxidation experiments. Maximum values are given for MACR and averaged values for the part of the experiment, when MACR was present, for the other parameters.

MACR	OH	NO <sub>x</sub>	NO	O <sub>3</sub>	RH	$j(\text{NO}_2)$	$T$	date
ppbv	$10^6 \text{ cm}^{-3}$	ppbv	pptv	ppbv	%	$10^{-3} \text{ s}^{-1}$	K	
14	2.5	0.8	90	40	40	4	301	11 Aug 2011
7	3.5	0.7	60	50	30	4	308	29 Aug 2012
9	3.5	0.6	70	40	45	4.5	302	6 Sep 2012

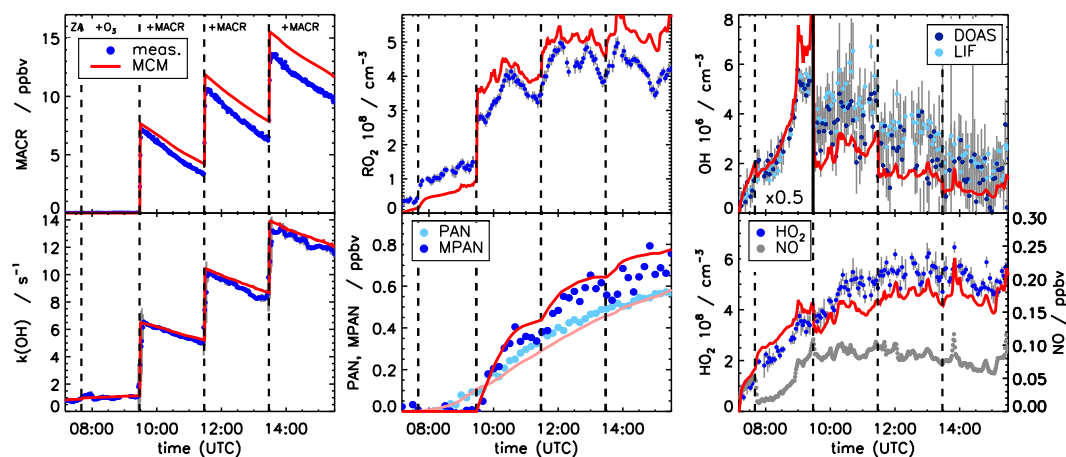


**Fig. 1.** Measured and modelled time series of MACR,  $k(\text{OH})$ , PAN, MPAN,  $\text{RO}_2$ ,  $\text{HO}_2$ , OH and NO for the experiment on 11 August 2011. OH concentrations during the less important initial part (“ZA”, “+O<sub>3</sub>”) of the experiment are scaled by a factor of 0.5. Model calculations applying MCM underestimate OH concentrations. Measured and modelled  $\text{HO}_2$  concentrations include a small fraction of  $\text{RO}_2$  radicals, which show up as an interference in the  $\text{HO}_2$  detection (less than 5 % of the entire concentration).  $\text{RO}_2$  radical concentrations shown here do not include the class of acyl peroxy radicals, which cannot be detected by the instrument.

observations, *Atmos. Chem. Phys.*, 11, 1269–1294, doi:10.5194/acp-11-1269-2011, 2011.

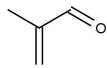
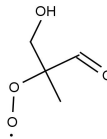
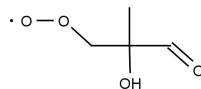
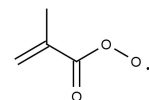
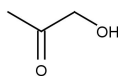
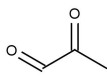
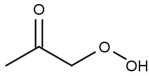
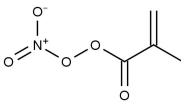
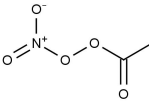
- 575 Wolfe, G. M., Crouse, J. D., Parrish, J. D., St. Clair, J. M., Beaver, M. R., Paulot, F., Yoon, T., Wennberg, P. O., and Keutsch, F. N.: Photolysis, OH reactivity and ozone reactivity of a proxy for isoprene-derived hydroperoxyenals, *Phys. Chem. Chem. Phys.*, 14, 7276–7286, doi:10.1039/C2CP40388A, 2012.

**Table 2.** Instrumentation for radical and trace gas detection during the MACR oxidation experiments.

	Technique	Time Resolution	$1\sigma$ Precision	$1\sigma$ Accuracy
OH	DOAS <sup>a</sup> (Dorn et al., 1995; Hausmann et al., 1997; Schlosser et al., 2007)	205 s	$0.8 \times 10^6 \text{ cm}^{-3}$	6.5 %
OH	LIF <sup>b</sup> (Lu et al., 2012)	47 s	$0.3 \times 10^6 \text{ cm}^{-3}$	13 %
HO <sub>2</sub> , RO <sub>2</sub>	LIF <sup>b</sup> (Fuchs et al., 2011)	47 s	$1.5 \times 10^7 \text{ cm}^{-3}$	16 %
$k(\text{OH})$	Laser-photolysis + LIF <sup>b</sup> (Lou et al., 2010)	180 s	$0.3 \text{ s}^{-1}$	$0.5 \text{ s}^{-1}$
NO	Chemiluminescence (Rohrer and Brüning, 1992)	180 s	4 pptv	5 %
NO <sub>2</sub>	Chemiluminescence (Rohrer and Brüning, 1992)	180 s	2 pptv	5 %
O <sub>3</sub>	Chemiluminescence (Ridley et al., 1992)	180 s	60 pptv	5 %
MACR	PTR-TOF-MS <sup>c</sup> (Lindinger et al., 1998; Jordan et al., 2009)	30 s	15 pptv	14 %
HONO	LOPAP <sup>d</sup> (Häseler et al., 2009)	300 s	1.3 pptv	10 %
HCHO	Hantzsch monitor (Kelly and Fortune, 1994)	120 s	20 pptv	5 %
CH <sub>3</sub> CHO	PTR-TOF-MS <sup>c</sup> (Lindinger et al., 1998; Jordan et al., 2009)	30 s	50 pptv	15 %
PAN	GC <sup>e</sup> (Volz-Thomas et al., 2002)	600 s	25 pptv	10 %
MPAN	GC <sup>e</sup> (Volz-Thomas et al., 2002)	600 s	25 pptv	20 %
Photolysis frequencies	Spectroradiometer (Bohn et al., 2005)	60 s	10 %	10 %

<sup>a</sup>Differential Optical Absorption Spectroscopy.<sup>b</sup>Laser Induced Fluorescence.<sup>c</sup>Proton-Transfer-Reaction Time-Of-Flight Mass-Spectrometry.<sup>d</sup>Long Path Absorption Photometer.<sup>e</sup>Gas Chromatography.

**Table 3.** Chemical structure of MACR and products from its oxidation with OH. Acronyms are taken from the MCM.

MACR (methacrolein)	
MACRO2	
MACROHO2	
MACO3	
ACETOL (hydroxyacetone)	
MGLYOX (methylglyoxal)	
HYPERACET (hydroperoxyacetone)	
MPAN (peroxy methacryloyl nitrate)	
PAN (peroxyacetyl nitrate)	

**Table 4.** Modification of MCM oxidation scheme for MACR. The “X”-mechanism adds generic recycling of OH via reaction of peroxy radicals with a compound X, which behaves like NO. The two cases of RO<sub>2</sub> isomerization produces additional OH via RO<sub>2</sub> isomerization with subsequent decomposition of the products.

	Reaction	Rate constant	Reference
X	RO <sub>2</sub> + X → HO <sub>2</sub>	$2.7 \times 10^{-12} \exp(360\text{K}/T) \text{ s}^{-1} \text{ cm}^3$	Hofzumahaus et al. (2009)
	HO <sub>2</sub> + X → OH	$3.45 \times 10^{-12} \exp(270\text{K}/T) \text{ s}^{-1} \text{ cm}^3$	
RO <sub>2</sub> isom. A	MACRO2 $\xrightarrow{1,5\text{-H-shift}}$ MGLYOX + OH + HCHO	0.008 s <sup>-1</sup>	Peeters et al. (2009)
RO <sub>2</sub> isom. B	MACRO2 $\xrightarrow{1,4\text{-H-shift}}$ ACETOL + OH + CO	$2.9 \times 10^7 \exp(-5300\text{K}/T) \text{ s}^{-1}$	Crounse et al. (2012)
	MACRO2 $\xrightarrow{1,5\text{-H-shift}}$ MGLYOX + OH + HCHO	0.0018 s <sup>-1</sup>	
	MACROHO2 $\xrightarrow{1,5\text{-H-shift}}$ HYPERACET + CO + HO <sub>2</sub>	0.5 s <sup>-1</sup>	

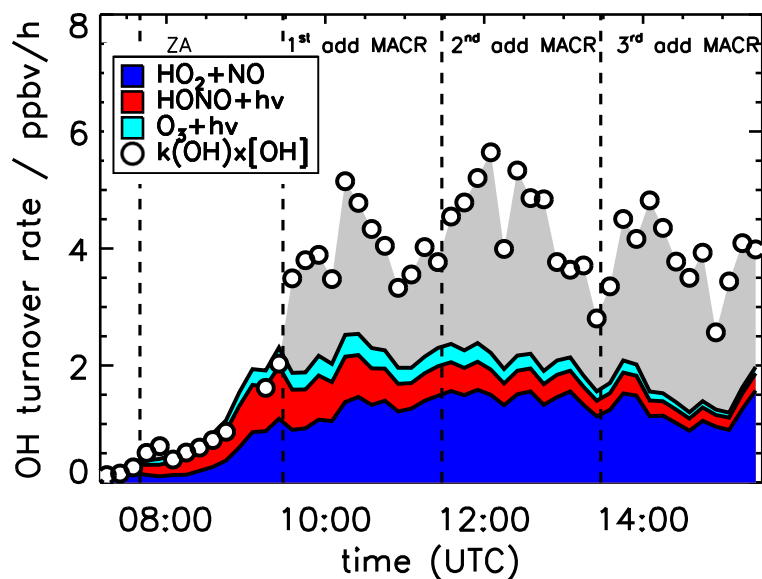


**Fig. 2.** OH budget for the experiment on 11 August 2011. Black circles give the turnover of the OH destruction rate calculated from measured OH concentrations (DOAS) and the measured OH reactivity. Coloured areas sum up the OH production from known sources ( $\text{HO}_2 + \text{NO}$  reaction,  $\text{O}_3$  and  $\text{HONO}$  photolysis), which can be calculated from measurements. □ cause of the short lifetime of OH, the production and destruction rates are expected to be equal at all times. The gray area denotes the difference between destruction and production rate. Whereas the OH budget is closed before the injection of MACR (“ZA”), on average half of the OH source is missed during MACR oxidation.  $\text{HO}_2$  measurements and calculations include a small interference from specific  $\text{RO}_2$  (see text for details).

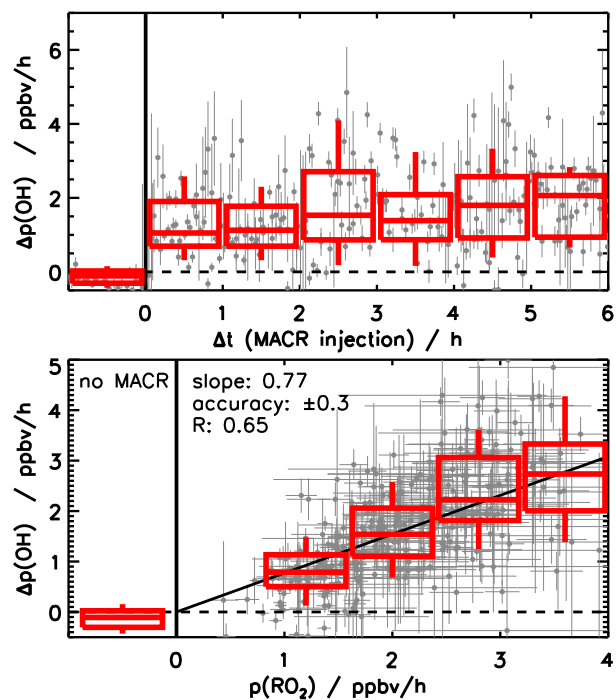


**Fig. 3.** Correlation between the missing OH source ( $\Delta p(\text{OH})$ ) and (1) the time that has elapsed since the first MACR injection (upper panel) and (2) production of  $\text{RO}_2$  from the reaction of MACR and OH (lower panel). Grey dots give individual data points with statistical errors for all three experiments (Table 1), boxes show 25 and 75 % and whiskers 10 and 90 % percentiles. The value of the linear correlation coefficient of  $R = 0.65$  shows the good correlation between the  $\text{RO}_2$  production from MACR and the missing OH source. The slope of a weighted linear fit (black line) suggests that on average 0.77 OH radicals are immediately recycled from  $\text{RO}_2$  for conditions of these experiments. The error of 0.3 is calculated from the accuracy of measurements.

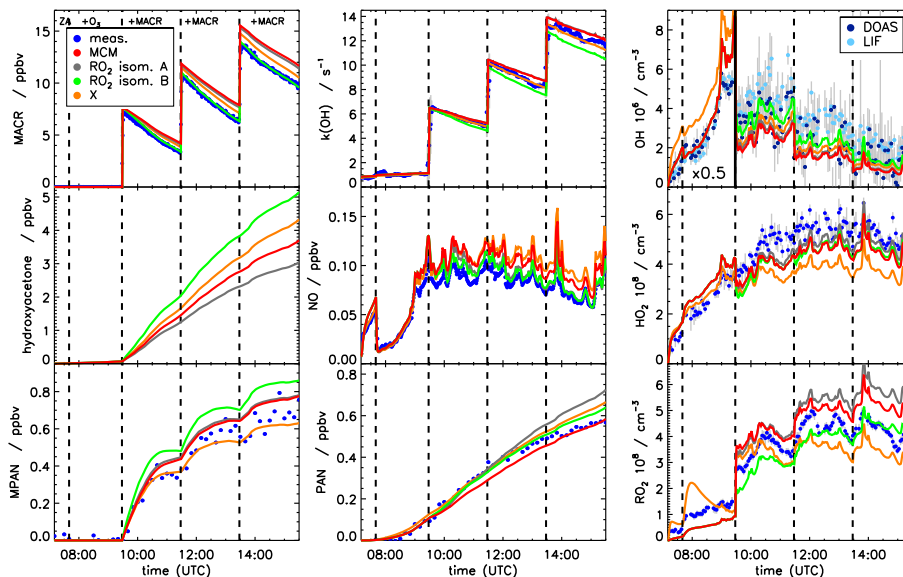


**Fig. 4.** Measured and modelled time series of MACR,  $k(\text{OH})$ , PAN, MPAN,  $\text{RO}_2$ ,  $\text{HO}_2$ , OH and NO for the experiment on 11 August 2011. OH concentrations during the less important initial part of the experiment are scaled by a factor of 0.5. Different model runs were performed applying the pure MCM, MCM with two additional  $\text{RO}_2$  isomerization reaction schemes (case A and B, see Table 4), and MCM with additional generic OH recycling (“X”) with an NO equivalent of 50 pptv. Only calculated hydroxyacetone concentrations are shown, because it was not measured during experiments.

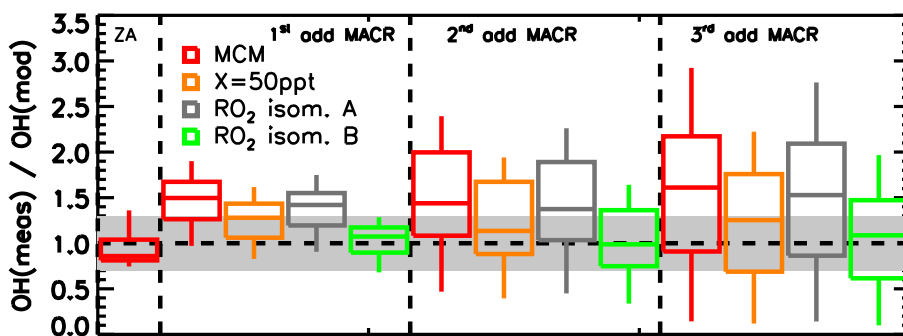


**Fig. 5.** Ratio of measured (DOAS) to modelled OH concentrations for the four parts of the experiment on 11 August 2011 applying different model approaches: MCM, MCM with additional generic OH recycling (“X”), and MCM with additional  $\text{RO}_2$  isomerization schemes (case A and B, see Table 4). The grey shaded area gives the range of agreement of modelled and calculated OH concentrations that is achieved in reference experiments.



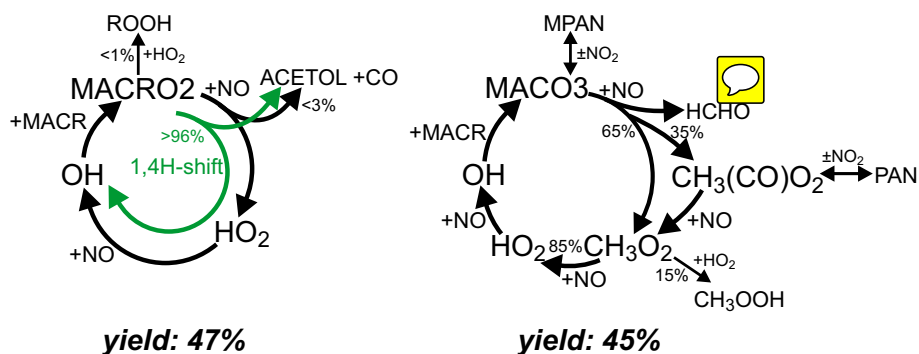


**Fig. 6.** Schematics of radical recycling from the reaction of MACR with OH taken from MCM (black arrows) showing the reactions which were of importance for conditions of these experiments. H-atom abstraction of the CHO group in MACR leads to the formation of an acyl peroxy radical (MACO<sub>3</sub>: yield 45%), whereas OH addition to the C=C double bond forms two hydroxyalkoxy radical isomers (RO<sub>2</sub>: MACRO<sub>2</sub>, yield 47%, and MACROHO<sub>2</sub>, yield 8% not shown here). Green arrows indicate the 1,4-H-shift reaction of MACRO<sub>2</sub> (Crouse et al., 2012) (the less important 1,5-H-shift is not shown here). Branching ratios are given for conditions of the experiment on 11 August 2011 (NO=90 pptv, HO<sub>2</sub>=5 × 10<sup>8</sup> cm<sup>-3</sup>, T = 301 K), if the fast unimolecular reaction is included.